ExoMars 2020 Cruise GNC formal verification of stability and robustness

Carlos Ardura*, Joost Veenman*, Cristina Recupero**, Antonio Pagano**, Nuno Silva***

* SENER INGENIERIA Y SYSTEMAS S.A.
Severo Ochoa 4 – PTM, 28760 Tres Cantos, Madrid, Spain, {carlos.ardura, joost.veenman}@sener.es

** DEIMOS SPACE SLU
Ronda de Poniente, 19, 28760 Tres Cantos, Madrid, Spain {cristina.recupero, antonio.pagano}@deimos-space.com

*** DEIMOS ENGENHARIA SA
Av. D. Joao II, No. 41, 1998-023 Lisboa, Portugal, nuno.silva@deimos.com.pt

Abstract
In the scope of the ExoMars 2020 mission, this paper addresses the formal analysis and verification of the cruise GNC with as main focus the certification of the control loops in terms of stability and robustness. In particular, it is shown how the main cruise GNC control loop can be modelled as a so-called linear fractional transformation (LFT) model, while explicitly including parametric and dynamic uncertainties such as MCI parameters, un-modelled dynamics, delay, estimation errors, etc. Subsequently, it will be demonstrated by means of the μ-tools that the structured singular value (SSV) or μ-theory can be adopted for the systematic verification and certification of robustness of the uncertain system.

1. Introduction

The ExoMars programme 2016-2020 is the result of a broad cooperation between the European Space Agency (ESA) and the Russian Space Agency (Roscosmos) with as main purpose to investigate the Martian environment and to demonstrate key flight & in-situ enabling technologies paving the way for the future Mars sample return mission. The programme consists of two missions to Mars that are scheduled for launch in 2016 and 2020 respectively.

The 2016 mission was composed of a trace gas orbiter (TGO) and an entry, descent and landing demonstrator module (EDM), also known as the Schiaparelli. The TGO carries scientific instruments to detect and study atmospheric trace gases such as methane, while the EDM contains a sensor suite to evaluate the lander's performance during the entry, descend, and landing as well as sensors to study the Martian environment at the landing site. On the other hand, the 2020 mission includes a rover equipped with a drill and a suite of other instruments dedicated to exobiology and geochemistry research.

Within this programme, SENER is involved in various projects. For the 2016 mission SENER was in charge of: 1) the front shield separation mechanism; 2) the surface platform structures and separation mechanisms, which includes the crush-structure that absorbs the energy of the impact of the landing; 3) the development of the special check-out equipment (SCOE) for the guidance, navigation and control (GNC) subsystem of Schiaparelli; 4) and the quality assurance activities of the NOMAD instrument software. On the other hand, for the 2020 mission, SENER is in charge of: 1) the development of three different mechanisms that are part of the drill system that is integrated in the Rover to obtain samples of the Martian soil (i.e. extension rods, drill translation group, and positioner translation group); 2) the umbilical release mechanism ; 3) the solar panel attachment and deployment mechanisms; 4) the development of the GNC-SCOE for the whole mission including cruise and entry phase.

Finally, SENER is participating in the ExoMars 2020 cruise GNC analysis and functional verification support project, which is being carried out by DEIMOS (prime contractor) and SENER (subcontractor) for Thales Alenia Space Torino (TASI) and ESA. The main goal of this project is to perform an independent GNC functional and performance

C. Ardura, J. Veenman, C. Recupero, A. Pagano, N. Silva

verification, which includes the definition of the verification plan as well as the subsequent execution thereof by means of formal and simulation based analysis techniques. For the latter a functional engineering simulator and a cruise GNC prototype were developed.

Within the scope of the latter project, this paper addresses the formal analysis and verification of the cruise GNC controller with as main focus the certification of the control algorithm in terms of stability and robustness. The cruise GNC ensures the correct attitude and trajectory control along the Earth to Mars journey from launcher separation up to the descent module release. The formal (i.e. analytical) stability analysis of a spin-stabilised attitude control system is challenging and requires advanced modelling and analysis techniques for a proper certification. Indeed, the problem comprises a multi-variable feedback control system which includes, among other things, dynamic coupling effects, actuator and measurement delay, estimation errors, as well as parametric and dynamic uncertainties such as mass, centre of mass, and inertial (MCI) parameter variations and un-modelled dynamics.

An important approach for the verification of stability and robustness in the presence of the previously mentioned characteristics is the framework of linear fractional transformations (LFT), which facilitates the modelling of uncertain control system interconnections as well as the systematic verification of robust stability in the presence of parametric and dynamic uncertainties by means of structured singular value (SSV) theory [1], [2], [3], [4]. The corresponding tools are readily available in MATLAB's robust control toolbox [5], [6].

The paper is organised as follows. Fist, a brief qualitative overview of the ExoMars 2020 mission and the cruise GNC is provided in Section 2 and 3 respectively. Subsequently, the paper continues in Section 4. Starting with the formulation of the nonlinear model of the spinning spacecraft, it is demonstrated how to systematically verify and guarantee stability and robustness of the ExoMars 2020 cruise GNC algorithms by means of the LFT framework and SSV theory. In particular, it will be shown that robustness can be guaranteed in the presence of dynamic coupling effects, actuator and measurement delay, estimation errors, MCI parameter variations and un-modelled uncertainties. The paper is concluded in Section 5 with some final remarks and conclusions.

2. Exomars mission overview

The 2020 ExoMars mission, which is led by Thales Alenia Space as prime contractor, consists of an ESA spacecraft composite (SCC), which will be launched by a Roscosmos Proton launcher. The SCC includes a carrier module (CM) and a descent module (DM), which are developed under ESA and Roscosmos responsibility respectively. The latter transports a surface station and a rover module (RM), while the CM facilitates the nine-month cruise phase of the SCC up to the arrival at Mars, where the DM is released from the CM. The CM will then break up and burn out in the Martian atmosphere, while the DM will perform its entry, descent and landing (EDL) on the Martian surface. After the successful landing, the RM is deployed on the Martian surface to accomplish its science and technology objectives. Here the corresponding strategy is to:

- land in an "ancient" location that possesses high exobiological potential for past life signatures;
- collect well preserved samples, free of oxidation and radiation damage, at different sites using the RM drill system;
- conduct an integral set of measurements that will provide reliable evidence for or against the existence of a range of bio-signatures for a nominal lifetime of 218 sols (~7 Earth months).
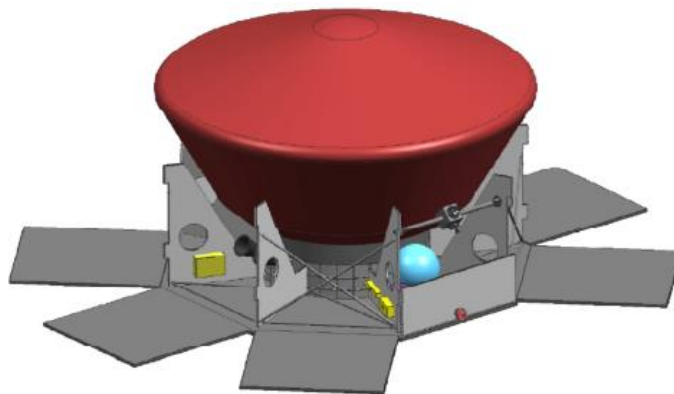
Figure 1: EXM 2020 Spacecraft Composite (image credit: TASI)

3. Cruise GNC overview

The SCC cruise GNC ensures that the trajectory and the attitude control of the SCC, needed for communication, power generation, and fine pointing during DM release during all mission phases from launcher separation up to the DM release, are carried out correctly. In addition, it ensures that the SCC's spin rate is actively controlled at 2.75 rpm about the principal axis of inertia (close to the SCC x-axis) during the cruise phase. Even though the spin-rate is relatively high, the selected star tracker unit will allow attitude determination at this angular rate with the required performances. The following requirements drive the cruise GNC design:

- Spin stabilized SCC
- High level of autonomy in relation to manoeuvres execution
- Pointing with the medium/low gain antennae (MGA/LGA), depending on mission phase and GNC mode
- Pointing strategy towards Sun or Earth depending on mission phase
- Accurate pointing at DM release for EDL mission initialization
- Fail safe and fail operational settings defined depending on mission phase criticality

The CM is equipped with two Sun detection sensors (SDS) and two star-trackers (STR) in cold redundancy, while the on-board computer (OBC), the two inertial measurement units (IMU) in cold redundancy, and the ground communication system (TM/TC) are located in the DM such that they are available for both the cruise as well as the EDL phase. This fact implies also that, after separation, the carrier is no longer capable to perform any "fine" attitude or trajectory determination and control. The SCC actuators consist of two sets, nominal and redundant, of 8 hydrazine thrusters. The thrusters are mounted such that forces and torques can be generated in any direction.

The attitude estimation is performed by a gyro-stellar Kalman filter. In case of short-term unavailability of the star tracker, the attitude is propagated by integration of the gyro data. The nominal attitude control during cruise brings the SCC x-axis pointing to the Sun in the first phase (about 50 days) to ensure sufficient power generation from the solar arrays and communication via the LGA. In the second phase (about 200 days), when Sun/SCC/Earth aspect angle is limited, the spin axis points towards the Earth in order to ensure communication with the MGA at higher distances.

In case of major anomalies, following sensor and actuator reconfigurations, the SCC autonomously enters a safe pointing attitude, making use of SDS sensors and gyros as main attitude sensors. The safe attitude ensures power generation and minimal communication with Earth stations; this level of autonomy can be maintained for several days.

The SCC cruise GNC will execute several trajectory correction manoeuvres (TCM). During these ΔV manoeuvres, the IMU accelerometers are used to integrate the SCC acceleration and to shut-off the reaction control system's (RCS) thrust once the target ΔV is reached. These measurements are also used for trajectory control purposes to autonomously detect and correct any deviation from nominal trajectory as a consequence of attitude manoeuvres or external disturbances.

In summary, the cruise GNC implements the following modes:
- Spin-up mode (SUM)
- Sun/Earth/inertial pointing mode (SPM/EPM/IPM)
- Delta-V mode (DVM)
- Pre-separation mode (PSM)
- Stand-by mode (SBM), Safe mode (SM), Survival mode (SVM)

3.1. Cruise GNC algorithm

An important driver for the cruise GNC design is simplicity. To this end, all the GNC modes rely on the same control architecture, sharing the same interfaces; they are configured differently depending on the particular GNC mode.

The GNC guidance and navigation functionalities provide the estimated SCC state deviation with respect to the reference SCC state and the estimated SCC MCI properties to the GNC controller that provides corrective actions at a frequency of 2 Hz. In turn, the controller provides the force and torque commands as well as the thruster heating requests to the RCS system (by means of on/off times). In addition, the GNC controller implements the estimation of the remaining propellant mass and provides information flags on the correct tracking/execution of the manoeuvres to the GNC manager. To this end, the GNC controller consists of the following functionalities:

- **Mode manager**: This function configures the control functionalities depending on the GNC mode/sub-mode
- **Attitude control**: This function computes the torque control commands needed for attitude control
- **ΔV-control**: This function computes the force control commands needed for trajectory control.
- **SCC inverse dynamics**: This function accounts for the gyroscopic terms of the SCC dynamics
- **Dispatching**: This function computes the RCS thruster on-times commands from the force-torque requests.

C. Ardura, J. Veenman, C. Recupero, A. Pagano, N. Silva

3.2. Stability requirements and verification approach

The verification of the stability requirements was carried out by means of formal and simulation based analysis techniques. As discussed in Section 4, the formal robustness analysis is based on the μ-tools that can be used for the systematic analysis of stability and performance properties of uncertain feedback interconnections [1], [2], [3], [4]. The use of these advanced techniques (rather than a more classical approach) was foreseen in the GNC requirement specification as some of the scenarios cannot be easily treated by means of classical techniques.

The simulation based analysis techniques rely on the use of a nonlinear high fidelity functional engineering simulator developed by DEIMOS [8]. The approach is primarily considered for GNC performance verification consisting of an extensive Monte Carlo campaign. On the other hand, its use in relation with the stability requirements is twofold:

1. Validate the linearized models of the GNC controller, the SCC plant, and the system feedback interconnection
2. Cross-check the predictions of the formal analysis to assess the potential conservativism of the applied methods

In addition, sensitivity analyses on the FES were performed for those (uncertain) parameters for which the formal robustness analysis revealed potential criticalities. Note that the functional engineering simulator includes the SCC flexible modes mainly due to deployable solar arrays and the liquid slosh of the fuel inside the tanks.

4. Stability analysis

Let us now proceed with the stability analysis. To properly assess the behaviour of the closed-loop system it does not suffice to rely on classical analysis approaches (e.g. checking the gain- and phase-margins). Indeed, the classical techniques are mostly restricted to the analysis of single-input single output (SISO) systems and do not allow to systematically incorporate uncertainties, while the nature of the system under consideration is multi-input multi-output (MIMO) and includes various sources of uncertainties. This calls for a more advanced way forward which offers the capability to address these concerns. One such approach is the LFT/μ-framework [1], [2], [3], [4] which allows to systematically verify the stability properties of uncertain MIMO systems as will become clear in the sequel.

As discussed, the stability analysis of the cruise phase consists of various GNC modes. Among others, it is possible to perform the following actions:

1. **Spin-up/down**: The SCC cruise GNC is capable of both increasing and decreasing the SCC's spin-rate in order to spin-stabilize the spacecraft after launcher separation at a certain angular rate and to de-spin the vehicle for slew execution in survival mode.
2. **Cruise**: After the spin-up phase, the SCC cruise GNC maintains a constant spin-rate, which is actively controlled throughout most of the cruise phase.
3. **TCMs and ΔV corrections**: On several occasions, a ΔV-manoeuvre needs to be performed in order to adjust the transfer orbit trajectory and to ensure that Mars is correctly reached.
4. **Slew/Search**: A slew/search manoeuvres are frequently performed to change the SCC's orientation to keep Earth pointing along the trajectory and/or to establish Earth-, Sun-, or inertial-pointing. Note that since the SCC is spin stabilised it maintains a fixed pointing of the spin-axis in an inertial reference frame.

In this paper, we restrict our attention to the formal verification of the cruise phase, which includes most of the relevant technical topics (i.e. the ΔV and the slew/search manoeuvres are automatically covered as these actions rely on the same feedback control law, while applying a smoothly varying feedforward reference profile).

4.1. Robustness analysis framework

As mentioned above, the LFT approach together with the μ-tools offer the possibility to systematically verify if an uncertain system is robustly stable [1], [2], [3], [4]. This proceeds as follows.

In a first step, it is key to obtain a so-called LFT model of the nonlinear feedback interconnection. Such representations consist of a nominal (closed-loop) plant P and an uncertainty block Δ, which is defined by the diagonal repetition of all modelled uncertainties and which is assumed to be confined to some bounded (i.e. stable) linear time-invariant (LTI) set Δ with $0 \in \Delta$. The main idea is illustrated in Figure 2.

In addition, we consider LFT models that have so-called generalised disturbance inputs (e.g. tracking reference (r), external disturbance (d), and noise inputs (n)), as well as generalised performance outputs (i.e. tracking error (z_1), control/plant outputs (z_2/z_3)).
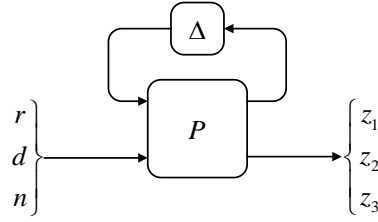
Figure 2: Linear fractional representation of the uncertain system interconnection

If partitioning P as

$$P = \begin{pmatrix} P_{11} & P_{12} \\ P_{21} & P_{22} \end{pmatrix}, \tag{eq. 1}$$

with the dimensions of the individual blocks being compatible with Δ, then the LFT defined by P and Δ is given by:

$$P \star \Delta := P_{22} + P_{21}\Delta(I - P_{11}\Delta)^{-1}P_{12}. \tag{eq. 2}$$

An LFT is said to be well-posed if $(I - P_{11}\Delta)^{-1}$ exists and is proper for all $\Delta \in \boldsymbol{\Delta}$. In addition, it is assumed that the nominal closed-loop system (i.e. P_{22}, which is obtained for $\Delta = 0$) is stable. Obtaining LFT models is facilitated, for example, by powerful tools that are readily available in MATLAB's robust control toolbox.

Given the LFT model representation, the task of verifying robust stability has now been reduced to checking if $(I - P_{11}\Delta)^{-1}$ is stable for all of the modelled uncertainties $\Delta \in \boldsymbol{\Delta}$. To do so, in this paper, we rely on the computation of the so-called structured singular values (SSV) by means of the μ-tools [4]. This proceeds as follows.

Let us consider complex matrices that have the same structure as Δ:

$$\Delta_{\rm c} = {\rm diag}\big(\delta_1^r I, \dots, \delta_l^r I, \delta_1^c I, \dots, \delta_m^c I, \Delta_1^f I, \dots, \Delta_n^f I\big) \in \mathbb{C}^{n_p \times n_q} \tag{eq. 3}$$

where

1. $\delta_i^r \in \mathbb{R}$, $i = 1, \dots, l$, are real parameters with $|\delta_i^r| < 1$;
2. $\delta_j^c \in \mathbb{C}$, $j = 1, \dots, m$, are complex parameters with $\left|\delta_j^c\right| < 1$;
3. $\Delta_k^f \in \mathbb{C}^{* \times *}$, $k = 1, \dots, n$, are full complex matrices with $\left\|\Delta_k^f\right\| < 1$;

If denoting the set of all these complex matrices by $\boldsymbol{\Delta}_c$, then the structured singular value of the complex matrix $P_c \in \mathbb{C}^{n_q \times n_p}$ with respect to the set of structured complex matrices $\boldsymbol{\Delta}_c$ is defined as:

$$\mu_{\boldsymbol{\Delta}_{\rm c}}(P_c) = \frac{1}{\sup\{r \geq 0 : \det(I - P_c\Delta_c) \neq 0 \quad \forall \Delta_c \in r\boldsymbol{\Delta}_c\}}. \tag{eq. 4}$$

This leads to the following result [4]: Let P_c be a complex matrix and $\boldsymbol{\Delta}_c$ an arbitrary set of (structured) complex matrices. Then the inequality

1. $\mu_{\boldsymbol{\Delta}_{\rm c}}(P_c) \leq r_u$ holds if and only if $\det(I - P_c\Delta_c) \neq 0$ for all $\Delta_c \in r_u^{-1}\boldsymbol{\Delta}_c$;
2. $\mu_{\boldsymbol{\Delta}_{\rm c}}(P_c) > r_u$ holds if and only if $\det(I - P_c\Delta_c) = 0$ for some $\Delta_c \in r_u^{-1}\boldsymbol{\Delta}_c$.

Let us now return our attention to the uncertain system interconnection in Figure 3 and observe that the interconnection is robustly stable if $(I - P_{11}\Delta)$ has a stable inverse for all $\Delta \in r_u^{-1}\boldsymbol{\Delta}$, which in turn holds if and only if

$$\mu_{\boldsymbol{\Delta}_{\rm c}}\big(P_{11}(i\omega)\big) \leq r_u \quad \forall \omega \in \mathbb{R} \cup \{\infty\}. \tag{eq. 5}$$

Hence, robust stability is achieved for all $\Delta \in \boldsymbol{\Delta}$ if $r_u \leq 1$. This is an exact characterization of robust stability for the feedback interconnection under consideration. Unfortunately, the exact computation of the SSV is in general hard, which enforces to resort to the computation of upper- and lower-bounds. This is what is done in the robust control toolbox of MATLAB.

C. Ardura, J. Veenman, C. Recupero, A. Pagano, N. Silva

4.2. Attitude dynamics

To perform the robustness analysis it is key to first formulate a dynamics model that represents the behaviour of the spinning satellite. In particular, let us consider the attitude dynamics, which can be described by Euler's equation as:

$$J\frac{d\omega(t)}{dt} = T_{ext}(t) - \omega(t) \times \big(J\omega(t)\big). \tag{eq. 6}$$

Here $T_{ext}(\cdot) \in \mathbb{R}^3$ denotes the external torque, $J \in \mathbb{R}^{3\times3}$ the spacecraft moment of inertia matrix, and $\omega(\cdot) \in \mathbb{R}^3$ the spacecraft angular velocity with respect an inertial reference frame expressed in body frame coordinates.

To be able to analyse the stability of the closed-loop system by means of the μ-tools, it is essential to obtain a linear model. Since the spacecraft is spinning with an almost constant and regulated spin-rate, $\omega_s \in \mathbb{R}$, we proceed by introducing a rotating reference frame whose x-axis coincides with the spin-axis of the spacecraft's inertial frame in order to express the angular velocity as $\omega = \eta + R\xi$. Here η denotes the angular velocity of the spacecraft with respect to the rotating reference frame expressed in the body frame, $\xi = \mathrm{col}(\omega_s, 0,0)$ the angular velocity of the rotating reference frame with respect to the inertial reference frame and expressed in the rotation reference frame, and R is a rotation matrix that maps reference frame coordinates into the body frame. Hence, the last matrix represents the attitude deviation of the spacecraft with regard the rotating reference frame. This allows to linearize the nonlinear equations of motion about the rotating reference frame in order to obtain a linearized state-space model that explicitly depends on the spin-rate ω_s:

$$\begin{pmatrix}\dot{\theta}(t) \\ \dot{\psi}(t)\end{pmatrix} = \begin{pmatrix}0 & I_3 \\ A_{21}(\omega_s) & A_{22}(\omega_s)\end{pmatrix}\begin{pmatrix}\theta(t) \\ \psi(t)\end{pmatrix} + \begin{pmatrix}0_{3\times3} \\ J^{-1}\end{pmatrix}u(t), \qquad y(t) = \begin{pmatrix}\theta(t) \\ \psi(t)\end{pmatrix}. \tag{eq. 7}$$

Here the states $\theta = \mathrm{col}(\theta_x, \theta_y, \theta_z)$ and $\psi = \mathrm{col}(\psi_x, \psi_y, \psi_z)$ respectively denote the angle and angular velocity, while $u(\cdot) \in \mathbb{R}^3$ is the external torque input and $y(\cdot) \in \mathbb{R}^3$ the output of the linearized system, which is equal to the state.

Since the state θ_x is not controlled, since it can be decoupled from the rest of the system, we instead consider the following decoupled state-space realisation for the analysis of the SCC x-axis pointing stability:

$$G: \{\dot{x}(t) = A(\omega_s)x(t) + Bu(t), \qquad y(t) = x(t). \tag{eq. 8}$$

This state space representation is obtained by applying the state transformation $T_5 = (0_{5\times1} \quad I_5)$ such that $x = \mathrm{col}(\theta_y, \theta_z, \psi_x, \psi_y, \psi_z)$.

As a final step, the obtained linearized model was validated against the nonlinear one by means of applying steps and sinusoidal to the inputs, while comparing the outputs. These results are not shown here.

4.3. Nonlinear and linearized controller

To continue, the to-be-analysed controller consist of a linear feedback law and a nonlinear feedforward compensator. The feedback law is defined by a simple PD control action, while the nonlinear feedforward compensator actively cancels the gyroscopic torques $\omega \times (J\omega)$. The controller can be modelled as follows:

$$y_c(t) = J\big(k_p T_2 e_\theta + k_d e_\omega\big) + \omega \times (J\omega), \tag{eq. 9}$$

Here $y_c(\cdot) \in \mathbb{R}^3$ is the control output, $e_\theta(\cdot), e_\omega(\cdot) \in \mathbb{R}^3$ the angular and angular velocity control errors respectively, k_p and k_d the proportional and derivative control gains, and $T_2 = (0_{2\times1} \quad I_2)$. As before, the nonlinear term can be linearized about the rotating reference frame. This yields the linearized controller K:

$$K: \Big\{y_c(t) = (JK_{fb} \quad K_{ff}(\omega_s))\begin{pmatrix}u_{fb}(t) \\ x(t)\end{pmatrix}, \qquad u_{fb} = \mathrm{col}(e_{\theta_y}, e_{\theta_z}, e_{\psi_x}, e_{\psi_y}, e_{\psi_z}). \tag{eq. 10}$$

Here $e_{\theta_i} = \theta_{r_i} - \theta_i$, $i = y, z$ and $e_{\psi_j} = \psi_{r_j} - \psi_j$, $j = x, y, z$ denote the tracking error signals with θ_{r_i} and ψ_{r_j} being the reference signals for the angle and angular velocity respectively.

4.4. Closed-loop system interconnection

In a next step, given the plant G and the controller K, let us proceed by considering the cruise control system interconnection as shown in Figure 3. Here, respectively, r, d and n denote the reference, external disturbance and

noise inputs, while z_1, z_2, and z_3 denote the tracking error, control, and plant performance outputs. These signals are dimension compatible with G, K.
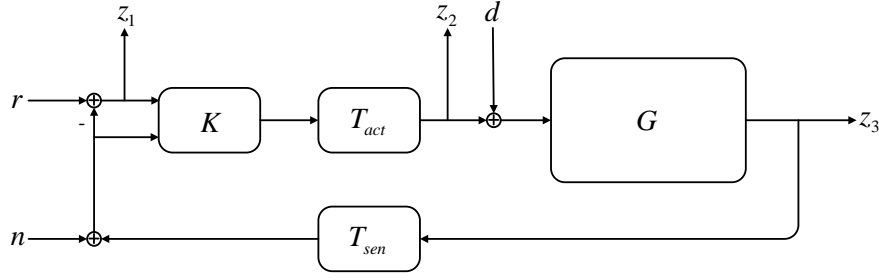
Figure 3: Control interconnection

The system interconnection is augmented by the actuator and sensor models T_{act} and T_{sen} respectively, which are given by:

$$T_{act}(s) = e^{-s\tau_{act}} \frac{\alpha_{act}}{s+\alpha_{act}} I_3, \ T_{sen}(s) = e^{-s\tau_{sen}} \frac{\alpha_{sen}}{s+\alpha_{sen}} I_5. \tag{eq. 11}$$

These are low-pass filters with a cut-off frequency equal to the sampling frequency, which define the constants α_{act}, and α_{sen}, while τ_{act} and τ_{sen} denote the delay times that are present in the actuator and sensor channel respectively. Clearly, these models are simplified and of low fidelity. However, they are sufficiently representative to proceed with the formal verification. In the following section it is shown how to include uncertainties in the control system interconnection in order to facilitate the robustness analysis.

4.5. Introducing uncertainties

4.5.1. Parametric uncertainty descriptions

For the robustness analysis, let us observe that various parameters, such as the moment of inertia matrix J are not precisely known. Within the robust control framework such parameters are called uncertainties, which can be easily incorporated in the system interconnection shown in Figure 3 as follows.

First, let us recall that the moment of inertia matrix, J, scales linearly with the mass, $m \in [m_{bol}, m_{eol}]$, where m_{bol} and m_{eol} denote the begin-of-life and end-of-life mass respectively. By taking $m_0 = 0.5(m_{bol} + m_{eol})$ and $m_d = 0.5(m_{bol} - m_{eol})$ the nominal mass can be expressed as:

$$m_{nom} = m_0 + m_d \delta_m, \qquad \delta_m \in [-1,1]. \tag{eq. 12}$$

Here δ_m denotes the normalized mass parameter, which, in the robustness analysis will be assumed an uncertainty. It is emphasized that even though this parameter is varying in time, it varies slowly enough to assume it to be time-invariant (which is a requirement for the μ-analysis). In addition, note that the mass is not exactly known on-board the SCC. If m_u denotes the maximum deviation of the mass with respect to the nominal mass, m_{nom}, the total mass can be expressed as:

$$m = m_0 + m_d \delta_m + m_u \delta_{mu}, \qquad \delta_m, \delta_{mu} \in [-1,1]. \tag{eq. 13}$$

In the same fashion, it is possible to express the uncertain moment of inertia matrix as:

$$J = \left(1 + \frac{m_d}{m_0}\delta_m + \frac{m_u}{m_0}\delta_{mu}\right) \begin{pmatrix} (1 + \delta_{xx}w_{xx})J_{0,xx} & \delta_{xy}J_{xy} & \delta_{xz}J_{xz} \\ \delta_{xy}J_{xy} & (1 + \delta_{yy}w_{yy})J_{0,yy} & \delta_{yz}J_{yz} \\ \delta_{xz}J_{xz} & \delta_{yz}J_{yz} & (1 + \delta_{zz}w_{zz})J_{0,zz} \end{pmatrix}. \tag{eq. 14}$$

Here $\delta_{ij} \in [-1,1]$, $i,j \in \{x,y,z\}$, while $J_{0,xx}, J_{0,yy}, J_{0,zz}$ are obtained by averaging the begin-of-life and end-of-life inertia values of the diagonal elements of J, while $w_{xx} = w_{yy} = w_{zz}$ denote the relative size of the uncertainty in the diagonal elements of J. This allows to obtain the nominal and uncertain moment of inertia matrix along the cruise trajectory.

C. Ardura, J. Veenman, C. Recupero, A. Pagano, N. Silva

To continue, the spin rate is also slowly varying about its nominal reference value with some minimum and maximum value $\omega_s \in [\omega_{s,min}, \omega_{s,max}]$. As we did for the mass, we can take $\omega_{s,0} = 0.5(\omega_{s,max} + \omega_{s,min})$ and $\omega_{s,d} = 0.5(\omega_{s,max} - \omega_{s,min})$ to obtain $\omega_s = \omega_{s,0} + \omega_{s,d}\delta_s$ with $\delta_s \in [-1, 1]$.

In addition to the latter uncertainty descriptions, the controller takes estimated information on the parameters J and ω_s as input to scale the control gains according to the mission state. Since the estimations are not exact, this introduces extra unknowns that can be assumed as uncertainties. Indeed, the estimated inertia $\hat{J}$ can be related to the one appearing in the plant as $\hat{J}_{ij} = (1 + \widehat{w}_{ij}\hat{\delta}_{ij})J_{ij}$, $i, j \in \{x, y, z\}$. Here $\hat{\delta}_{ij} \in [-1,1]$ are the normalised estimation uncertainties, while the constants $\widehat{w}_{ij}$ capture the magnitude of the estimation error. Here it is noted that the estimation errors of the off-diagonal elements of J are typically significantly larger that the diagonal ones.

Finally, the spin rate ω_s is also affected by estimation errors. As before, this can be expressed as $\widehat{\omega}_s = (1 + \widehat{w}_s\hat{\delta}_s)\omega_s$ where $\hat{\delta}_s \in [-1,1]$ and $\widehat{w}_s$ again captures the magnitude of the estimation error.

In summary, the closed-loop control interconnection is subject to 16 parametric uncertainties that all will be taken into account in the robustness analysis.

4.5.2. Dynamic uncertainty descriptions

In addition to parametric uncertainties, the control system is also subject to dynamic uncertainties. Indeed, the models T_{act} and T_{sen} are subject to actuator and sensor model uncertainties and also include the delay terms $e^{-s\tau_{act}}$ and $e^{-s\tau_{sen}}$, which need to be reformulated in order to be able to include the effect in the robustness analysis. To this end, we replace T_{act} and T_{sen} with the following multiplicative uncertainty models:

$$T_{act}(s) = \left(1 + w_{act}(s)\delta_{act}(s)\right)\left(1 + w_{a,del}(s)\delta_{a,del}(s)\right)\frac{\alpha_{act}}{s+\alpha_{act}}I_3, \quad \|\delta_{act}\|_\infty < 1, \quad \|\delta_{a,del}\|_\infty < 1,$$

$$T_{sen}(s) = \left(1 + w_{sen}(s)\delta_{sen}(s)\right)\left(1 + w_{s,del}(s)\delta_{s,del}(s)\right)\frac{\alpha_{sen}}{s+\alpha_{sen}}I_5, \quad \|\delta_{sen}\|_\infty < 1, \quad \|\delta_{s,del}\|_\infty < 1.$$

(eq. 15)

Here the terms $(1 + w_{act}(s)\delta_{act}(s))$ and $(1 + w_{sen}(s)\delta_{sen}(s))$ express the dynamic uncertainty of the actuators and sensors by means of δ_{act} and δ_{sen}, which are unknown and possibly infinite dimensional transfer functions that are bounded in the H_∞-norm by one. The uncertainties are weighted over frequency by the high-pass filters $w_{act}(s)$ and $w_{sen}(s)$. In other words, the actuator and sensor models are assumed to be more accurate at low frequencies than at higher frequencies.

In addition to the dynamic uncertainties, T_{act} and T_{sen} are affected by delay. Since this effect cannot be directly taken into account in the robustness analysis (without introducing conservatism in the analysis), we proceed in the standard fashion by modelling it as an uncertainty (see e.g. [7]). To do so, the initial terms $e^{-s\tau_{act}}$ and $e^{-s\tau_{sen}}$ can be replaced by the multiplicative uncertainty models $(1 + w_{a,del}(s)\delta_{a,del}(s))$ and $(1 + w_{s,del}(s)\delta_{s,del}(s))$. Here $\delta_{a,del}$ and $\delta_{s,del}$ are also bounded in the H_∞-norm by one, while the weighing functions $w_{a,del}$ and $w_{s,del}$ should be chosen as $|e^{-i\omega\tau} - 1| \leq |w_{del}(i\omega)\delta_{del}(i\omega)| \leq |w_{del}(i\omega)||\delta_{del}(i\omega)| \leq |w_{del}(i\omega)|$ for all delay values $\tau \in [0, \tau_{max}]$ and for all $\omega \in [0, \infty]$. A μ-robustness analysis can then proceed in the usual fashion. See e.g. [7] for further details.

In summary, we have introduced all the relevant sources of uncertainties and so that we can proceed with the robustness analysis as summarized in the following section.

4.6. Robust stability analysis

Given the control system interconnection together with the uncertainty descriptions, it is now possible to obtain an LFT representation of the control system interconnection shown in Figure 3, by means of MATLAB's robust control toolbox (i.e. the "sysic" routine). This yields a representation as depicted in Figure 2, where P represents the nominal closed-loop system and where Δ denotes the main uncertainty block, which is defined by the diagonal repetition of all the modelled uncertainties:

$$\Delta = \text{diag}\left(\delta_m I, \delta_{mu}I, \delta_{xx}I, \cdots, \delta_{zz}I, \hat{\delta}_{xx}I, \cdots, \hat{\delta}_{zz}I, \delta_s I, \hat{\delta}_s I, \delta_{act}I, \delta_{a,del}I, \delta_{sen}I, \delta_{s,del}I\right).$$

(eq. 16)

Given the LFT representation it is now straightforward to compute the robust stability margin by means of performing the μ-analysis. This yields the information shown in Figure 4. These are the computed lower- and upper-bounds of the SSV as a function of frequency. As can be seen, the largest SSV is approximately 0.68, which means that the robust stability margin is $\frac{1}{0.68} = 1.47$. In other words, we have formally verified that the system is robustly stable to all of the modelled uncertainties with a margin of 1.47.
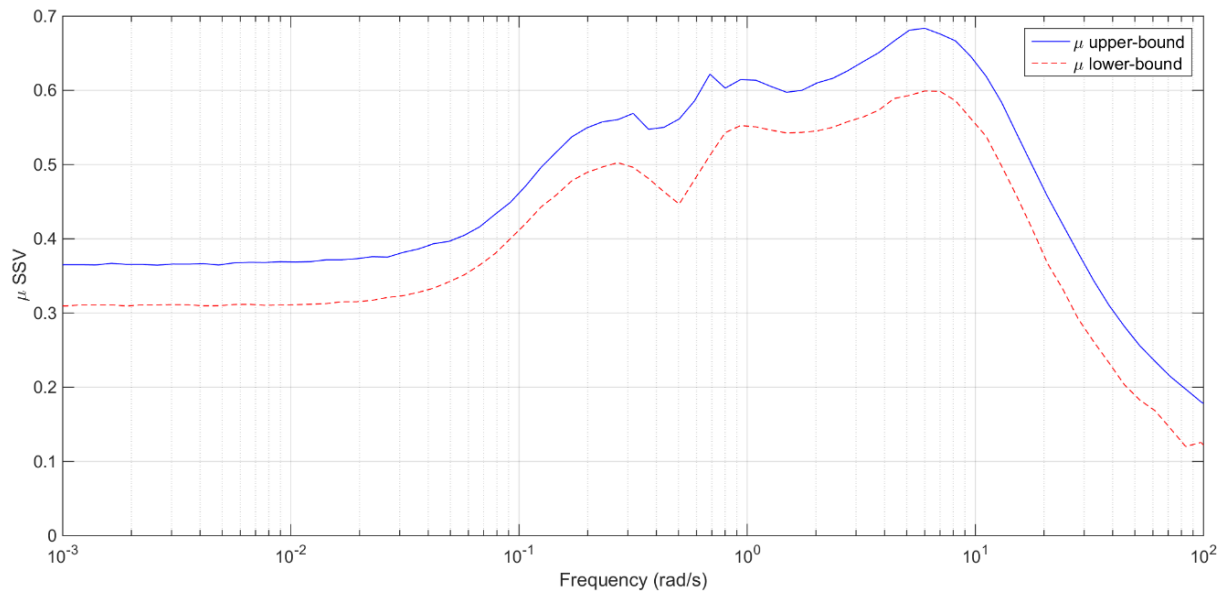
Figure 4: Computed structured singular values for the uncertain system including all modelled uncertainties

It is emphasized that the robustness analysis can be easily extended to include robust performance. However, this was outside the scope of the project. In addition, it is noted that a proper robustness analysis includes a sensitivity analysis, where the uncertain parameters are varied in order to detect to which of the modelled uncertainties the control system is most sensitive. To do so, let us first consider the case where all dynamic uncertainties are set to their nominal value. This yields the results shown in Figure 5. As can be seen, the SSV bounds are significantly lower in the frequency range starting from 0.1 rad/s and higher. From this (and other analysis that is not shown here) we can infer that the control system interconnection is not sensitive to the parametric uncertainties.

To further investigate this, let us again consider the full set of uncertainties, but now varying the maximum delay uncertainties as $\tau_{sen} = 0.5\tau_{max}$, $\tau_{act} = \tau_{max}$, and $\tau_{max} \in \{0, 0.125, 0.25, 0.375, 0.5\}$ seconds. This yields the results shown in Figure 6. As can be seen, the maximum SSV upper-bound (i.e. μ_{max}) degrades noticeably for increasing τ_{max}. However, in all scenarios robust stability is guaranteed, even in the case that the delay uncertainties exceed their maximum value with a factor of 2.
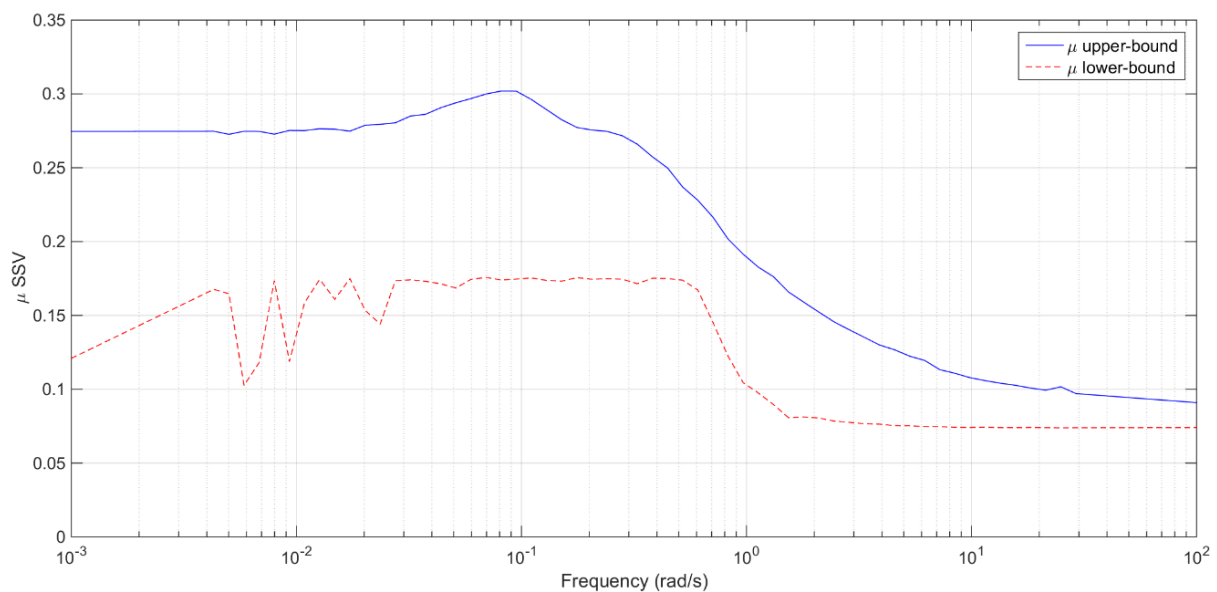
Figure 5: Computed structured singular values for the uncertain system including all parametric modelled uncertainties, while the dynamic uncertainties are set to their nominal value.

C. Ardura, J. Veenman, C. Recupero, A. Pagano, N. Silva
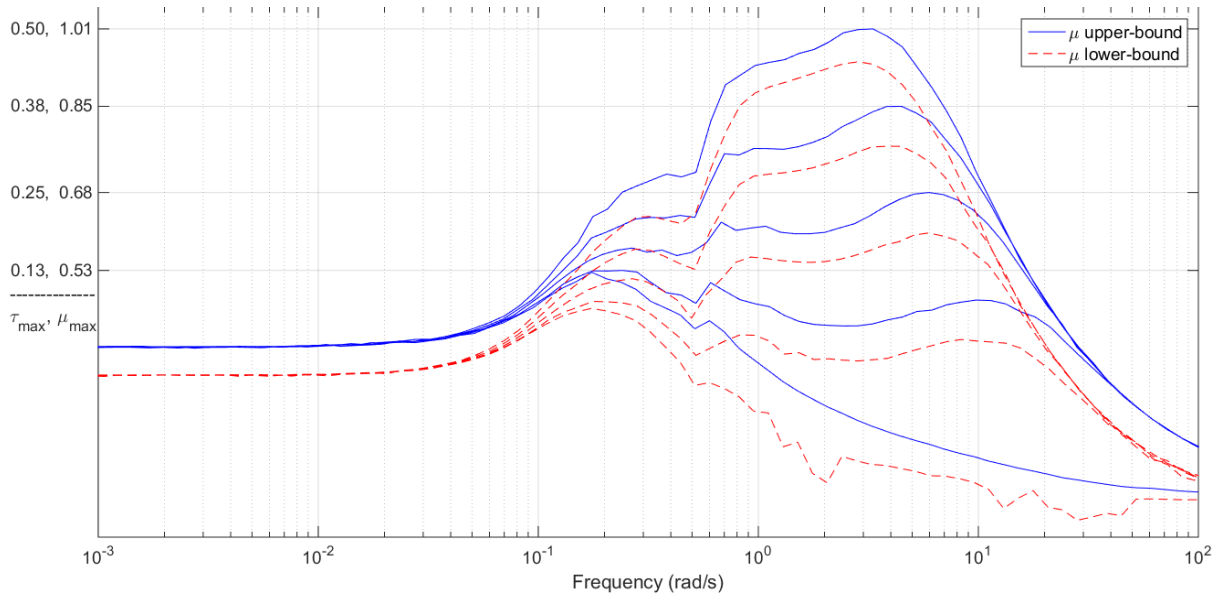
Figure 6: Computed structured singular values for the uncertain system including all modelled uncertainties, while varying the delay uncertainties with $\tau_{sen} = 0.5\tau_{max}$, $\tau_{act} = \tau_{max}$, and $\tau_{max} \in \{0, 0.125, 0.25, 0.375, 0.5\}$

5.   Final remarks and conclusions

In the scope of the ExoMars 2020 cruise GNC analysis and functional verification support project, a formal verification of was performed to certify the cruise GNC algorithms. In particular, in this paper, we have addressed one of the main scenarios: The robustness analysis of the cruise GNC phase (inertial-pointing).

In particular, we have shown how to derive a linear fractional transformation (LFT) model describing the control feedback interconnection. Subsequently, we have shown how to include all the relevant uncertainties that are present in the control feedback loop. Finally, given the LFT uncertainty model, a robustness analysis was performed by means of the μ-tools.

It was concluded that the cruise GNC is guaranteed to be robustly stable in the presence of all of the modelled uncertainties. In addition, a sensitivity analysis was performed in order to identify to which of the modelled uncertainties the control system is sensitive the most. This analysis revealed that the system is most sensitive to delay uncertainties (if compared to the other uncertainties). Nonetheless it was shown that control feedback interconnection can tolerate twice the amount of delay uncertainties without becoming unstable.

6.   Acknowledgements

7.   References

[1] S. Skogestad and I. Postlethwaite, Multivariable Feedback Control – Analysis and Design, John Wiley & Sons, Ltd., 2005.

[2] K. Zhou, J. Doyle and K. Glover, Robust and optimal control, Upper Saddle River, New Jersey: Prentive-Hall, Inc., 1996.

[3] G. Dullerud and E. Paganini, A Course in Robust Control Theory, Texts in applied mathematics, New York: Springer-Verlag, 1999.

[4] A. Packard and J. Doyle, "The complex structured singular value," *Automatica,* vol. 29, pp. 1251-1256, 1993.

[5] G. Balas, R. Chiang, A. Packard and M. Safonov, "Robust Control Toolbox," The MathWorks Inc., 2005-2008.

[6] G. J. Balas, J. C. Doyle, K. Glover, A. Packard and R. Smith, "mu-analysis and synthesis toolbox (μ-tools)," Mathworks Inc., 1991.

[7] J. Veenman, C. W. Scherer and H. Köroglu, "Robust stability and performance analysis based on integral quadratic constraints," *European Journal of Control,* vol. 31, pp. 1-32, 2016.

[8] C. Recupero, A. Pagano, N. Silva, C. Ardura, J. Veenman, "Analytical and simulation based V&V techniques applied to the ExoMars 2020 cruise GNC," in the proceedings of the 8th European Conference for Aeronautics and Space Sciences (EUCASS), 2019.